XXXVI Ibero-Latin American Congress on Computational Methods in Engineering
CILAMCE
Rio de Janeiro, 22-25 Nov 2015

# FEASIBLE TIME DOMAIN JACKET FATIGUE ANALYSES

**Said Fawad Mohammadi**

s.mohammadi@tuhh.de

**Nelson Szilard Galgoul**

nsg@nsg.eng.br

Universidade Federal Fluminense, Department of Civil Engineering, DNV GL Consultant

**Uwe Starossek**

starossek@tuhh.de

Hamburg University of Technology, Structural Analysis and Steel Structures Institute

**Paulo Maurício Videiro**

pmauricio@petrobras.com.br

Petróleo Brasileiro S.A.

***Abstract.*** *While many fixed offshore platforms in Brazil date back to the 1980's, inspections have shown that they can safely remain in service for a longer period than originally forecast. These inspections are costly and, therefore, have been minimized based on computational methods developed to assess the risk associated with structural fatigue failure. Early deterministic fatigue analyses were inaccurate and have thus been replaced by spectral fatigue techniques, which are considered a feasible method to determine the fatigue life. In spite of their wide recognition, the accuracy of these analyses is still unsatisfactory since they provide only a qualitative indication of the remaining service life. The most accurate way of determining the remaining fatigue life is a time domain analysis that simulates an irregular water surface, which so far has been too computationally demanding to be considered feasible. This paper contributes to the literature in two important ways. First, it proposes a novel approach for time domain fatigue analysis that drastically reduces the computational burden, while maintaining a high degree of accuracy. Second, this paper shows the impact that the main parameters have on the results and thus provides practical guidance on carrying out fatigue analyses in the time domain.*

***Keywords:*** *Life Extension, Fixed Platforms, Time Domain Analysis, Fatigue Analysis*

# 1 INTRODUCTION

Several jackets are operating in the Campos Basin, along the coast of Rio de Janeiro/Brazil, with the oldest ones installed in the 1980's. Experience has shown that the common reason for large-scale tubular structures to fail after such a long period of service life is due to fatigue (Marshall, 1992). Industry codes such as API (2007), DNVGL (2014) and ISO (2013) require an evaluation of the resistance against fatigue failure to ensure structural integrity. The fatigue analysis locates points with high risk of fatigue failure. Based on these indications inspection plans have to be set up, which can be quite costly. In this regard a distinction has to be made between shallow and deeper water inspections. Shallow water inspections up to a depth of 30m can usually be made by divers, whereas deeper water inspections require the use of Remote Operated Vehicles (ROVs), which increases the costs significantly. Inspecting an entire jacket structure is not economically feasible, which is why computational methods that can accurately determine locations of high risk of fatigue failure offer substantial cost saving potential.

The previously mentioned codes contain several methods for fatigue analysis among which the frequency domain approach (or spectral fatigue) is the most common for jacket design. Frequency domain analyses are computationally more efficient but are considered less accurate than solutions in the time domain (Naess & Moan, 2013). Nevertheless, computational constraints have made time domain fatigue analyses infeasible so far, because a single computation may require days to be completed. Time domain analyses for an extreme response have so far found application in systems such as TLP's and Spars (ABS, 2014), where dynamic response plays a larger role, and should be adopted for fixed structures as well if dynamic amplification becomes significant (Barltrop & Adams, 1991). Usually these analyses are simulating a short period of time whereas the paper presented here promotes the use of a time domain analysis for fatigue purposes, which requires simulating the entire service-life. Previous work has attempted to reduce the computational burden of time domain fatigue analyses (see e.g. Jia, 2008). However, the proposed approach of reducing the number of seastates by averaging the scatter diagrams, introduces unquantified errors into the analysis and should therefore be avoided.

This paper contributes to this literature in two important ways. For the case of offshore jackets in a first step a systematic study of the parameters required to perform a time domain analysis is provided which leads to a reduction of the computational burden by choosing appropriate parameter values. Results show that computation time still remains excessive even after optimal parameter choice. Therefore, in a second step, this paper proposes an approach that interpolates damage between seastates and thus substantially reduces computational effort required while maintaining a high level of accuracy.

The remainder of this paper is organized as follows. Chapter 2 shows the steps that are necessary to perform a common time domain fatigue analysis. Chapter 3 investigates the set of input parameters that lead to fatigue results within an acceptable error margin while reducing the time necessary to perform the fatigue assessment. Chapter 4 proposes a novel approach that shows that an interpolation of damage between the seastates is a valid option to avoid simulating all seastates. Finally, Chapter 5 concludes.

# 2 FATIGUE ANALYSIS IN THE TIME DOMAIN

## 2.1 Generating the irregular water surface

It is the objective of the time domain fatigue analysis to recreate the natural events that lead to fatigue failure. The natural events are recorded through measurements of the surface elevation, whose characteristics are captured by a power spectrum. The power distribution of each seastate contains information about which individual waves are associated to a specific height. From the original measurements, the information of the phase shift for each wave component is lost. The assumption is made that the water elevation can be defined as a stationary Gaussian random process with zero mean (Barltrop & Adams, 1991). For this case the power spectrum $S^{+}(\omega)$ and the height $h_j$ of a frequency bandwidth $\Delta\omega$ are related in the following way.

$$h_j = 2\sqrt{\int_{\omega_l}^{\omega_l+\Delta\omega} S^{+}(\omega)\,d\omega}\,, \tag{1}$$

where $S^{+}(\omega)$ represents a single-sided power spectrum and $\omega_l$ the lower bound of the frequency bandwidth (USFOS, 2010). The height $h_j$ of each component is used to generate a set of individual waves. These waves are then shifted randomly based on a uniform distribution with angles between 0 and 2π. This set of individual waves is superimposed through an inverse Fast Fourier Transform (FFT) to generate the irregular surface elevation as shown in Fig. 1.

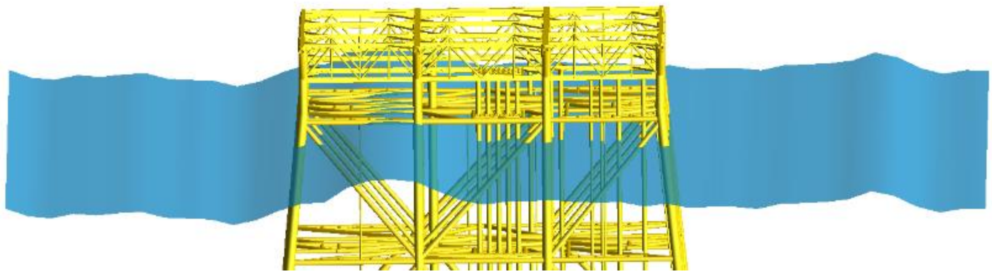

**Figure 1. Platform subjected to an irregular water surface**

The superimposed waves are used to determine the velocities and accelerations that the structure is subjected to. These values are required in Morison's equation (Morison, 1953) in combination with drag and inertia coefficients to determine the actual forces applied on the jacket structure (Sarpkaya, 2010).

## 2.2 Specifications of the sample platform

A sample platform is used to verify the parameters proposed for the time domain fatigue analysis. This platform has a total height of approximately 170m from the main deck to the mudline in a water depth of about 150m. The jacket has dimensions in the water plane of 60m by 40m. Jackets built in the 1980's, such as the one chosen for this paper, were anchored by piles driven through the platform legs. This solution is consistent with the hammer restrictions that were relevant at that time: hammers were operable only above water. The piles are modelled as equivalent beam elements, whose stiffness is derived from a full nonlinear pile-soil interaction analysis. The modules on the main deck of the topsides are simulated by point masses at the center of gravity of each module. The weight of the entire platform sums up to about 53.000t. The jacket and the steel structure at the topsides weigh approximately 26.000t while the remaining 27.000t belong to the aforementioned modules and additional equipment placed on the structure. Corrosion effects or material degradation over time are not taken into account in this paper. It is assumed that splash zone corrosion is protected by an increased wall thickness and that anode protection works efficiently for the rest. A viscous damping coefficient of 1.5% is used based on the recommendations of API (2007) and ISO (2013). The drag and inertia coefficients applied in this analysis are recommended by API (2007), which also recommends an increase of 6% due to appurtenances. Marine growth has been accounted for considering an increase of the outer diameter of the tubular members based on local data valid for the Campos Basin. The material is represented by a linear elastic model as recommended by ISO (2013) for fatigue assessment. The largest natural period of the sample platform is about 3.5 seconds, which is why dynamic effects are included (API, 2007).

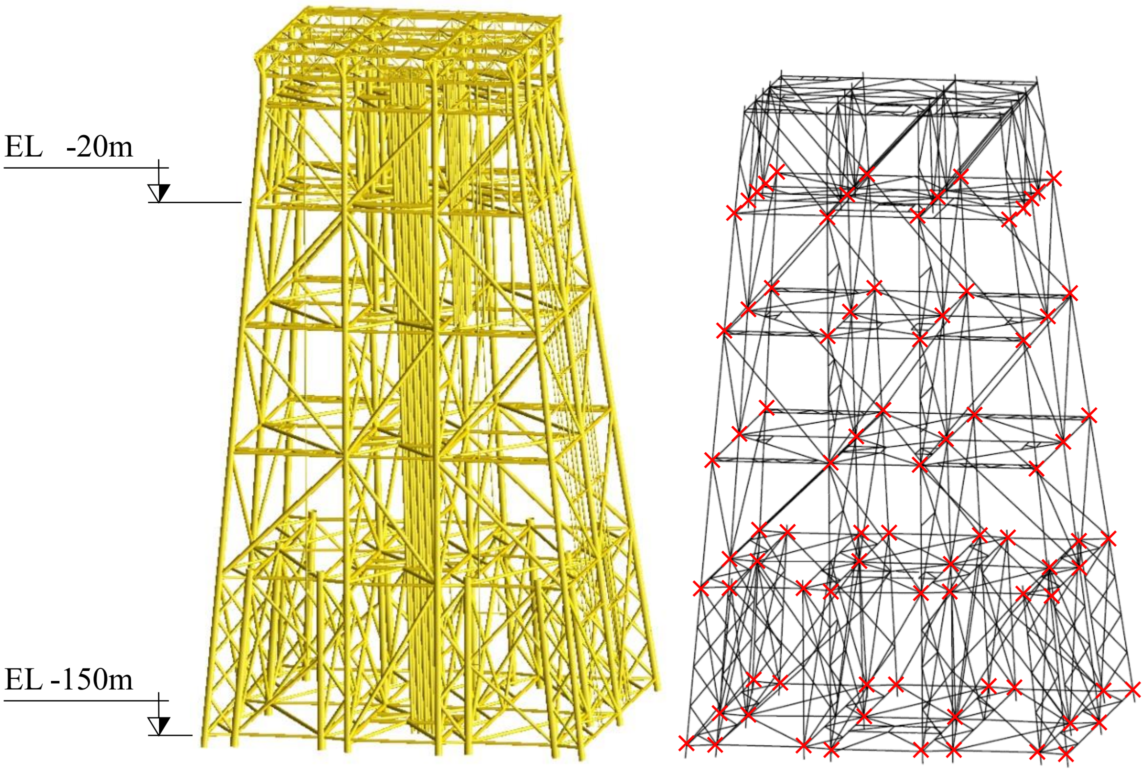


**Figure 2. Isometric view of platform on the left; analyzed joints marked on the right**

Since the focus of this paper is to identify locations of risk due to fatigue below the splash zone, Fig. 2 on the right indicates which joints are included in the analysis. These joints are considered crucial for the structural integrity of the platform. The platform consists of welded, tubular connections, which are commonly used for jackets. In the offshore environment the most common failures for tubular structures occur in the heat affected zone of the welds (Marshall, 1992). This occurs because welding generates residual stresses due to the uneven cooling process (Dowling, 1999) and changes in the microstructure that increase the probability of fracture at these locations (Anderson, 2005). In addition, the geometry of the weld causes high stress concentrations both at the chord and the brace side. This makes these locations the most probable places for a crack to occur or propagate (Lassen & Recho, 2006). For the analyses performed in this paper the stress concentration factors (SCF) are determined by the formulation derived by Efthymiou (1988).

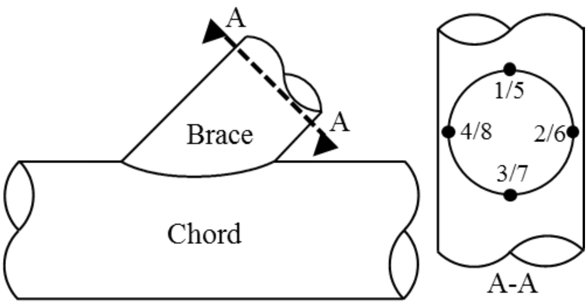


**Figure 3. Identification of hot spots on both brace and chord side**

The resulting stresses are determined for eight hot spots per tubular connection. As indicated in Fig. 3 there are a total of four hot spots at the chord and four hot spots at the brace side, where the fatigue damage is calculated. In the case of the sample platform the number of 93 joints results in 600 connections, with eight hot spots each.

## 2.3 Environmental data

The main driving force for fatigue in offshore jackets is the structural displacement due to wave action. Current and wind forces are usually neglected (ISO, 2013). In order to quantify the waves that occur at a given location, measurements of the surface elevation were performed and made available for this paper. Each measurement was conducted for three hours, which is considered long enough to generate an accurate power distribution of the surface elevation. Although the measurements of the long term period are not stationary, it is assumed that the short term measurement of three hours is (Naess & Moan, 2013). Table 1 provides a typical scatter diagram of the measured seastates for one direction. Each value represents the occurrence probability of the seastate. The parameters of peak period $T_p$ and significant wave height $H_s$ (Sorensen, 2006) are used to describe the power distribution, which is represented by a JONSWAP spectrum (Hasselmann, et al., 1973). The values for $H_s$ and $T_p$ are provided in intervals. In this paper typical Campos Basin scatter diagrams are used to perform the fatigue calculations which consist of a total of 331 seastates and eight directions ranging from 0° to 315° in 45° steps. The scatter diagrams of the two landside directions show only a few seastates that were measured.

**Table 1. Typical scatter diagram with service life fraction in [‰]**

| | | $T_p$[s] | | | | | | | | | | | |
|---|---|---|---|---|---|---|---|---|---|---|---|---|---|
| $H_s$[m] | | 3 | 4 | 5 | 6 | 7 | 8 | 9 | 10 | 11 | 12 | 13 | 14 |
| | | 4 | 5 | 6 | 7 | 8 | 9 | 10 | 11 | 12 | 13 | 14 | 15 |
| 0.5 | 1 | | | 0.1 | 0.2 | | | | | | | | |
| 1 | 1.5 | | 0.2 | 0.7 | 0.8 | 1.1 | 0.3 | 0.2 | 0.1 | | | | |
| 1.5 | 2 | 0.1 | 0.8 | 2.1 | 4.3 | 5.2 | 3.7 | 2.4 | | 0.3 | 0.1 | | |
| 2 | 2.5 | | 0.3 | 2.1 | 4.7 | 6.5 | 4.3 | 3.1 | 1.2 | 0.2 | | 0.1 | |
| 2.5 | 3 | | | | 0.9 | 1.7 | 2.1 | 1.1 | | | | | |
| 3 | 3.5 | | | | | | 0.5 | | | | | | |

## 2.4 Fatigue damage calculation

Among the several methods to determine the fatigue damage this paper uses the stress-based approach of comparing the applied number of cycles to the allowable number of cycles provided by an S-N curve. This curve defines the maximum number of cycles *N* that the tubular member can resist for a constant stress variation *S*. The S-N curve used in this paper is provided by DNVGL (2014) specifically for welded tubular joints. The applied number of cycles *n* and stress variations $\Delta\sigma$ for each analyzed seastate are determined through the Rainflow Algorithm (Dowling, 1999).

The Rainflow Algorithm does not differentiate between stress variations in the compressive or tensile regime. Beneficial effects that occur under compression like crack closure (Anderson, 2005) are not taken into account due to large residual stresses in the welds that reach up to yield (BSI, 2013) and which can lead to a continued stress state in the tensile regime. The assumption is made that for fatigue analyses of welded connections the nominal stresses are not sufficient to invert the stress state even if the nominal stresses are compressive (DNVGL, 2014). As a result each stress variation $\Delta\sigma$ presumably leads to a crack growth and is counted by the Rainflow Algorithm.

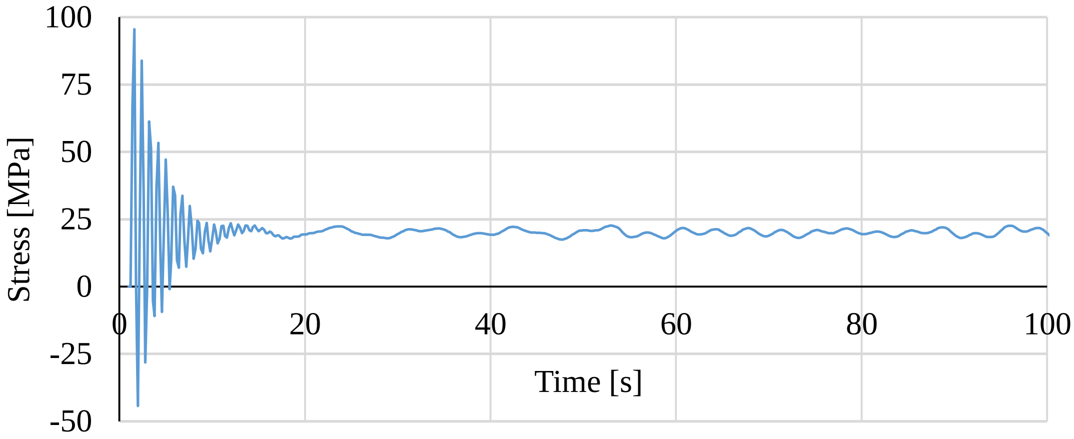


**Figure 4. Initiation phase of hot spot stress**

Figure 4 shows the stress of a hot spot that reacts very sensitively during the initiation phase. The large oscillations show how long the solution requires to reach the steady state. These large stress variations in the initiation phase would distort the results of the fatigue calculation. Therefore, a time interval of 20 seconds is used to reach the steady state after which the stress variations and cycles are counted by the Rainflow Algorithm. The total fatigue damage is calculated by linear summation assuming the validity of Palmgren-Miners rule (Palmgren, 1924).

$$D_{HotSpot} = \sum_i \frac{n_i}{N_i}. \tag{2}$$

The inverse of the total damage determined for a hot spot times the design life is defined as the fatigue life.

# 3 EVALUATION OF PARAMETERS FOR TIME DOMAIN FATIGUE

## 3.1 Overview of parameters influencing the runtime

There are several parameters that influence the time required to perform the analysis. The following parameters are significant:

- time step during the analysis
- number of frequencies used as components for the FFT
- sensitivity towards choice of seed
- simulated timeframe
- number of analyzed seastates

Although the choice of time step has a significant contribution to the required duration, the influence of this factor is not analyzed explicitly in this paper. The time step size needs to be small enough so as to accommodate the discretization of even relatively small waves into acceptable intervals (ISO, 2013). Thus for example a 2 second wave would need to be discretized into at least ten steps resulting in time steps of 0.2 seconds.

At the same time it is necessary to have a sufficient number of frequency components for the FFT to simulate accurately small deviations in the water surface. The phase shift of each component of the FFT is generated through a random number generator that requires a seed. The choice of seed has an impact when a large wave build-up is generated and when crests and troughs cancel each other out. Based on the assumption of a narrow banded process this pattern tends to repeat itself within a specific timeframe (Naess & Moan, 2013). The timeframe should guarantee a sufficient amount of wave build-ups which does not influence the average damage that is created.

This chapter investigates the sensitivity each aforementioned parameter has on the fatigue damage calculation. The results lead to a conclusion specifying which value for each parameter is acceptable for the case of offshore jackets. In order to quantify an acceptable error margin it is imperative to understand that several uncertainties are inherent in fatigue analyses, which is why fatigue damage should be considered as an estimate rather than an accurate value (API, 2007). While time domain analyses are already subject to fewer uncertainties than frequency domain analyses some uncertainties remain. Broadly speaking for the specific case of offshore jackets these are:

- assumptions due to wave action (stationary Gaussian process, applied wave theory)
- welding defects (residual stresses, changes in steel micro-structure)
- S-N curve assumptions (constant amplitude loading, loading-ratio)
- errors in SCF methodology
- number of applied cycles (Rainflow Counting)
- linear damage summation using Palmgren-Miners rule

In order to take these uncertainties into account the S-N curve is provided for a given confidence interval. The curve used in this paper lies at the mean minus two standard deviations of the performed experiments, meaning that 97.7% of the experiments exceeded the number of cycles that are defined by way of the S-N curve (DNVGL, 2014). Based on the impact that these uncertainties have on the fatigue damage, damage errors within ±50% can be considered acceptable. The following sensitivity analysis of the involved parameters will be judged for fatigue purposes only.

## 3.2 Sensitivity to water surface simulation

The number of frequencies used as components for the FFT increases proportionally to the amount of time required to perform the fatigue analysis. In other words, twice as many frequencies result in double the total time. Some guidance on the choice is provided by Chakrabarti (2005) who suggests values between 200 and 1000. In an example study Naess & Moan (2013) suggest the use of 100 frequencies for the range where waves have significant energy. To capture an extreme response for installation purposes DNV (2011) suggests using at least 1000 frequencies while for other purposes 100 frequencies are considered adequate. It seems obvious that for a jacket structure these indications vary too much, which is why the impact on the choice of number of frequencies used for FFT is further analyzed. In order to determine the impact of this parameter one seastate is analyzed for a variety of frequencies, ranging from 100 to 1000 with steps of 100. The results shown in Fig. 5 are obtained for several analyses with a duration of three hours using the same seed. The chosen seastate is characterized by a JONSWAP spectrum ($T_p$=7.5sec., $H_s$=2.25m, 180° direction) and has the highest fraction of life of the entire scatter diagram.

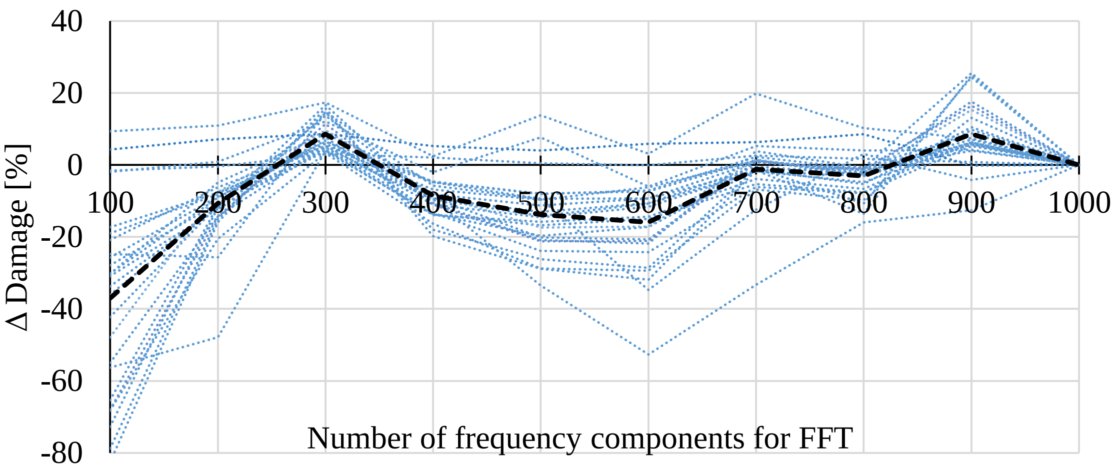


**Figure 5. Changes in damage due to different numbers of frequencies for one seastate**

Figure 5 shows the difference in the damage relative to the results obtained with the analysis that uses 1000 frequencies. The lines show the change in damage created for the worst 25 hot spots (blue lines) and the average over all hot spots (black line). The range in which the damage deviates is quite low but can lead to significant changes if it takes place in all 331 seastates. A difference can already be noted between 1000 and 900 frequencies, which is about 10% and seems acceptable. Below 200 frequencies this difference increases, which is why the following analyses are performed with 250 frequencies. In order to verify the global impact this number of frequencies has, all 331 seastates are analyzed with a simulated duration of one hour for 100, 250 and 500 frequency components. The result is shown in Fig. 6 similar to the previous graph.

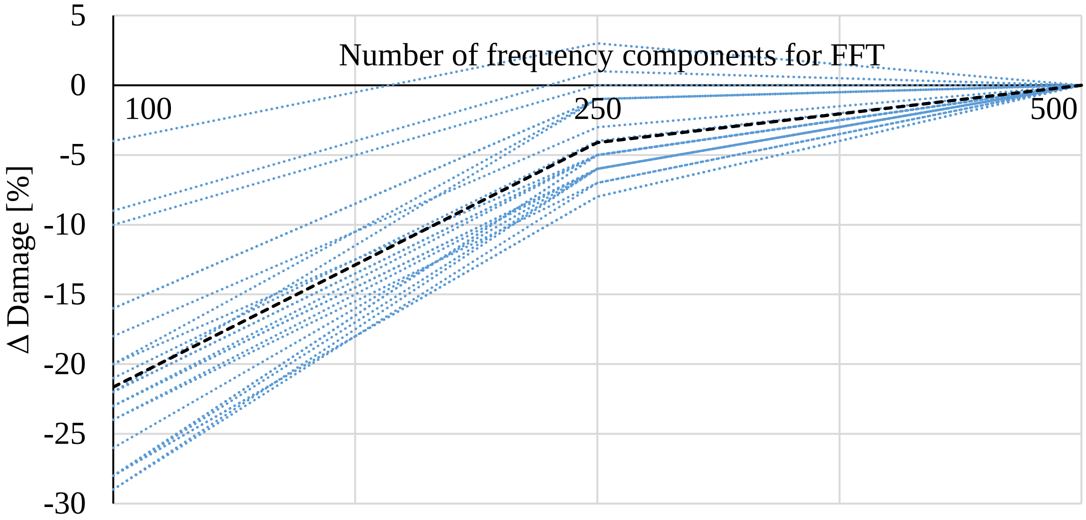


**Figure 6. Changes in damage due to different number of frequency components for all seastates**

Figure 6 shows that in the global model the difference in damage is similar to Fig. 5. The difference between 500 and 250 frequency components is marginal (±10%) while the damage below 250 frequencies starts to deviate (up to -30%) for the worst 25 hot spots.

## 3.3 Sensitivity to choice of random seed

The phase angle of each component of the FFT is randomly shifted based on a chosen seed. In order to determine the impact of the seed number on the final damage a total of 100 analyses of the same seastate are performed while varying the seed used for each analysis.

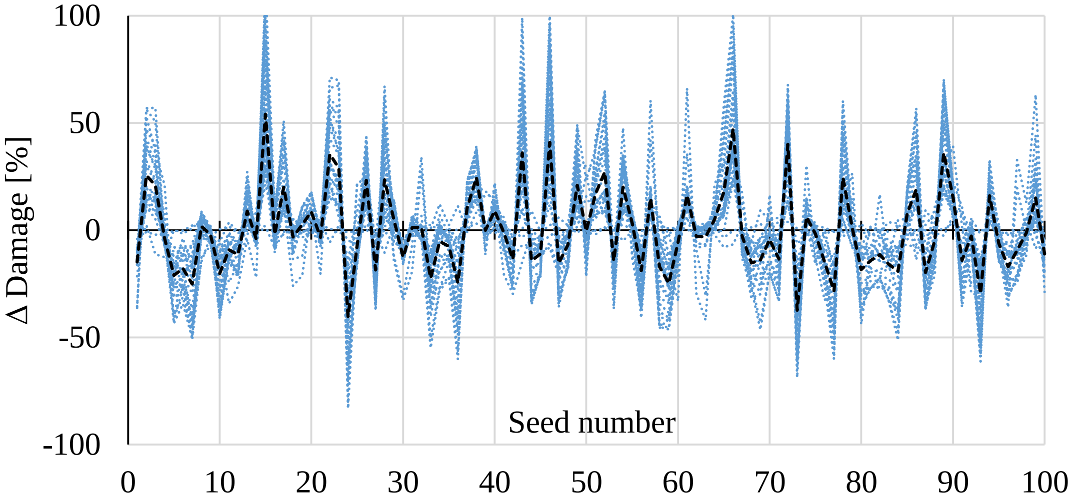


**Figure 7. Changes in damage due to different seeds, $T_p$=7.5sec., $H_s$=2.25m, 180° direction, 3h duration**

Figure 7 shows the difference in damage for the worst 25 hot spots (blue lines) and the average (black line). The determined damage values are compared to the average of the entire set. Changes of up to 50% on average are possible, which would be unacceptable if this were to occur numerous times. The distribution of the damage deviation is presented in Fig. 8.

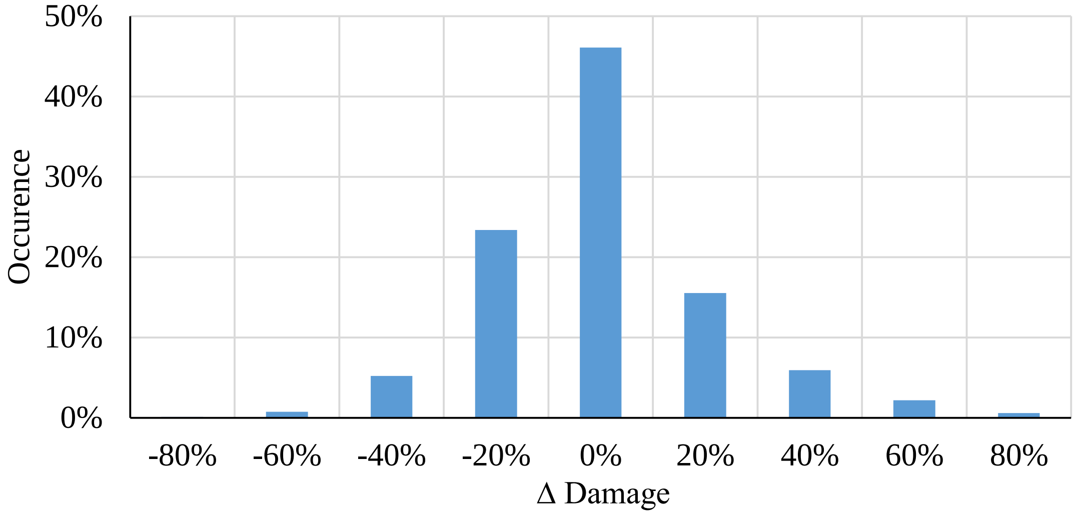


**Figure 8. Distribution over damage variation due to different seeds**

The large majority of the differences in damage are in the order of ±20%, which can be considered acceptable for fatigue analyses. It seems unlikely that for all 331 seastates the chosen seeds would all result in larger or smaller damage. The most probable case is that the majority will be within the ±20% regime and just a few outside this interval. In order to verify this assumption a total of four analyses are performed, where all 331 seastates are given a different random seed each. Figure 9 shows the difference in damage for the worst 25 joints (blue lines) and the average deviation (black line) of the damage among the four simulations.

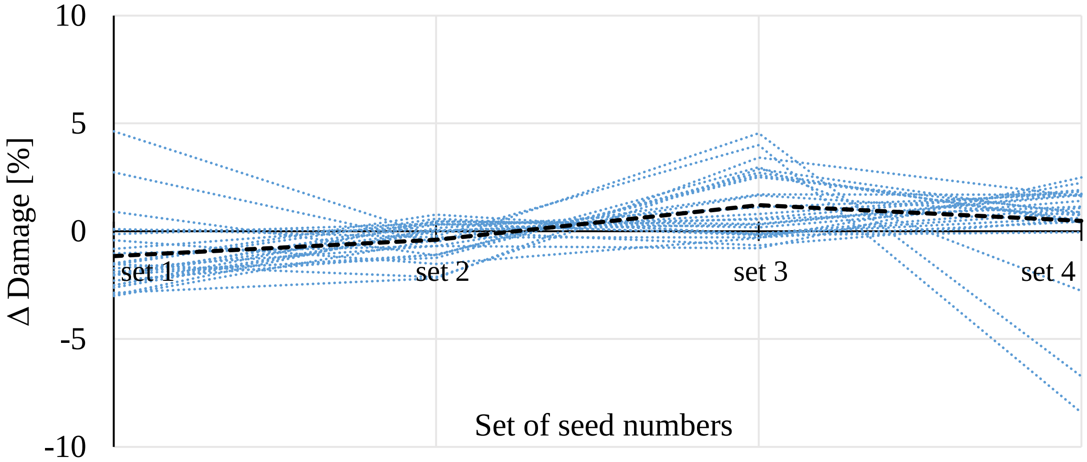


**Figure 9. Changes in damage due to different seeds for all 331 seastates, 1h duration**

The damage deviates little among the four analyses and remains below 10%. While there is a small chance that the choice of seed number can influence the damage of a single seastate as shown in Fig. 8, the impact on the analysis of all seastates is negligible. These results clearly show that across all seastates the impact of random seed numbers is marginal and therefore can safely be ignored for the remaining analyses.

## 3.4 Sensitivity towards duration of the simulated timeframe

It seems only natural to reproduce the surface elevation using the same duration of three hours but this becomes computationally infeasible. Reducing the simulated time will always entail a reduction of accuracy. The following graph shows the sensitivity towards a reduction of simulation time. The analyses are performed with 250 frequencies and the same seed for a specified seastate ($T_p$=7.5sec., $H_s$=2.25m, 180° direction).

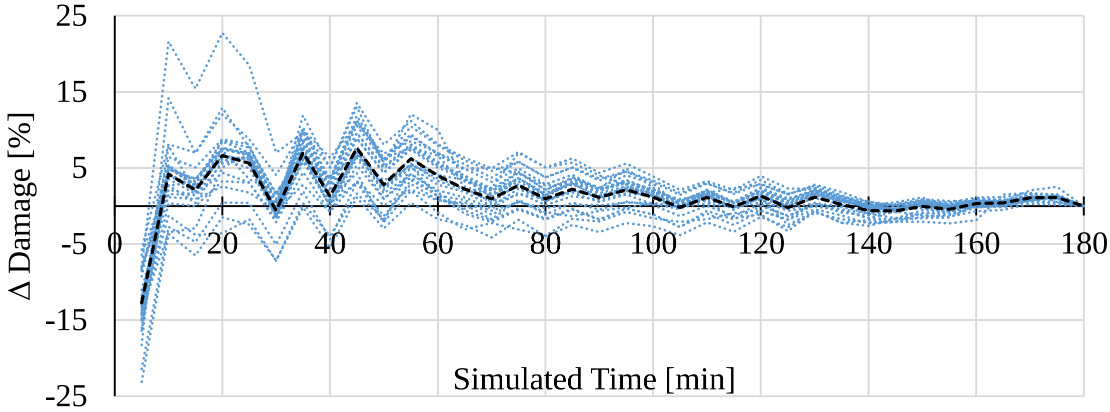


**Figure 10. Runtime and associated error due to changes in simulated time for one seastate**

Figure 10 shows how much the total damage of the worst 25 hot spots for the specified seastate deviates from the main analysis with a three hour duration. The blue lines represent the deviation of the damage of the worst 25 hot spots while the black line shows the average of the set. The simulated time is reduced in 5 minute steps from 180 minutes down to 5 minutes. Below a duration of 60 minutes the deviation starts to increase. Similar to the previous comparison of one seastate the impact on the damage deviation is determined if all 331 seastates are analyzed. The seed number is kept constant for this comparison while the duration is reduced from 180 minutes to 10 minutes in 10 minute steps. Again the damage of the worst 25 hot spots (blue lines) with the average (black line) is presented in Fig. 11.

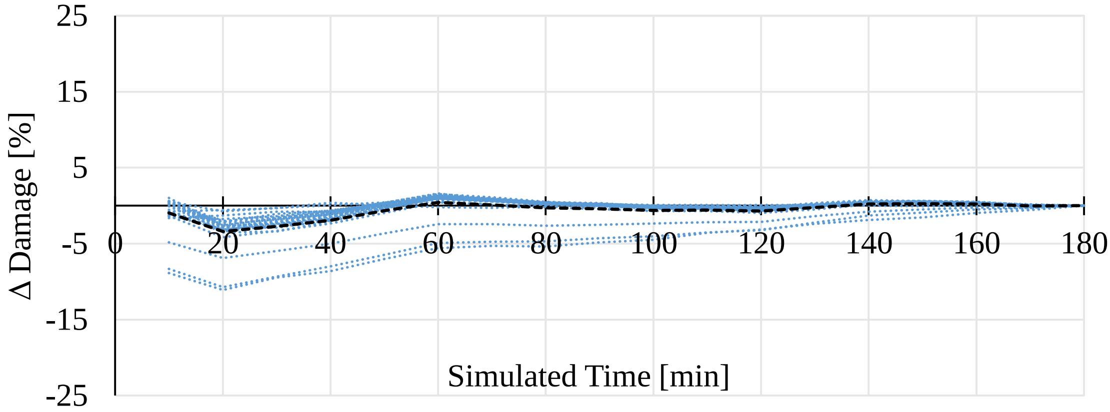


**Figure 11. Runtime and associated error due to changes in simulated time for all seastates**

The average results (black line) in Fig. 11 show that the deviation of the damage increases below a simulated time of 60 minutes. Therefore, in order to obtain an accurate set of results it can be justified to reduce the simulated time from three hours to one hour. This will reduce the required time to perform the analysis by a factor of three.

## 3.5 Time domain analysis of sample platform

For a given setting the sample platform is analyzed in the time domain. The setting is specified by:

- 0.2 seconds time step for the analysis
- a different set of random seeds is generated for each seastate
- three hour and one hour simulated time per seastate
- 250 frequencies used as components for the FFT
- all 331 seastates are analyzed

The markings in Fig. 12 indicate the worst hot spot of the joint. Only those hot spots are shown that have a fatigue life below 200 years, which would be the same as a design life of 50 years with a safety factor of four.

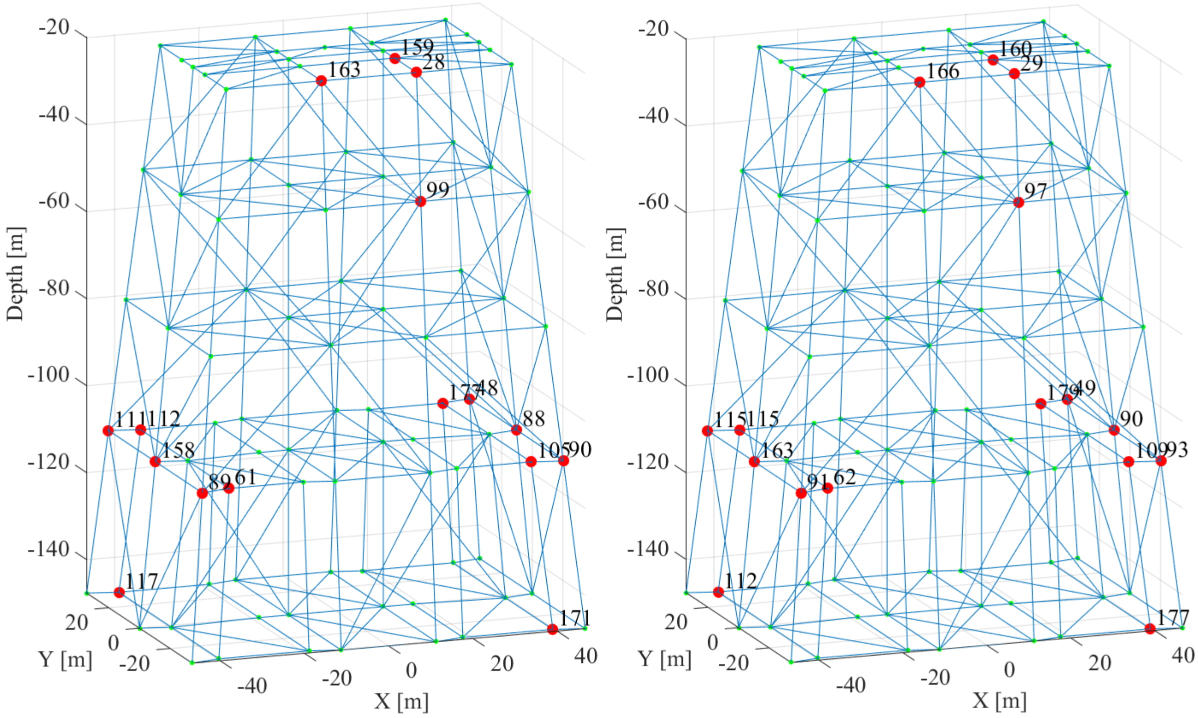


**Figure 12. Platform showing points with low fatigue life, duration 3h (left) and 1h (right) per seastate**

The lines that indicate the beams are not an accurate representation of the geometry and are just presented for orientation purposes. It can be seen that the joints, which show low fatigue life, are located on the skirt pile and leg bracing at elevation -109m. The joint with the lowest fatigue life is found at elevation -20m with a fatigue life of about 28/29 years.

Having chosen appropriate settings for all influential parameters, the computation of this specific case study still requires excessive time in order to complete. Further changes in the parameters would introduce errors in the analysis that even for fatigue considerations can become too large.

# 4 FATIGUE DAMAGE INTERPOLATION METHOD

## 4.1 Interpolating damage between seastates

The previously mentioned parameters (frequencies for FFT, simulated time) provide a reduction in computation time that is still not sufficient so as to make the analysis feasible in a design project. Therefore, this paper proposes a novel, interpolation-based approach.

In a time domain analysis all seastates that occur are supposed to be analyzed and the damage that is created at each hot spot should be determined. In order to propose an efficient interpolation method it is necessary to understand how damage varies with changes in $T_p$ and $H_s$. Assuming that all seastates in a chosen scatter have the same number of occurrences provides a clear indication of the variations. This is illustrated in Table 2, which shows the damage for one occurrence per year at the worst hot spot for a specific direction.

The values in the table are based on an analysis with a duration of three hours per seastate and 250 frequency components. The color scale ranging from blue with nearly no damage up to red with high damage suggests a trend which is indicated by the arrow.

**Table 2. Damage per year of worst hot spot, 0° direction**

| | $T_p$[s] | | | | | | | | | | | | |
|---|---|---|---|---|---|---|---|---|---|---|---|---|---|
| $H_s$[m] | 5.5 | 6.5 | 7.5 | 8.5 | 9.5 | 10.5 | 11.5 | 12.5 | 13.5 | 14.5 | 15.5 | 16.5 | 17.5 |
| 0.25 | 0.000 | 0.000 | 0.000 | 0.000 | 0.000 | 0.000 | 0.000 | 0.000 | 0.000 | 0.000 | 0.000 | 0.000 | 0.000 |
| 0.75 | 0.007 | 0.003 | 0.001 | 0.001 | 0.001 | 0.002 | 0.002 | 0.002 | 0.001 | 0.002 | 0.001 | 0.001 | 0.001 |
| 1.25 | 0.038 | 0.021 | 0.012 | 0.013 | 0.014 | 0.014 | 0.014 | 0.013 | 0.012 | 0.010 | 0.010 | 0.009 | 0.008 |
| 1.75 | 0.083 | 0.050 | 0.035 | 0.032 | 0.032 | 0.031 | 0.031 | 0.029 | 0.026 | 0.025 | 0.022 | 0.020 | 0.018 |
| 2.25 | 0.153 | 0.091 | 0.063 | 0.055 | 0.058 | 0.056 | 0.052 | 0.050 | 0.045 | 0.042 | 0.038 | 0.035 | 0.031 |
| 2.75 | 0.233 | 0.141 | 0.098 | 0.089 | 0.086 | 0.084 | 0.081 | 0.076 | 0.072 | 0.065 | 0.059 | 0.053 | 0.047 |
| 3.25 | 0.360 | 0.211 | 0.151 | 0.126 | 0.126 | 0.122 | 0.119 | 0.109 | 0.104 | 0.093 | 0.085 | 0.077 | 0.067 |
| 3.75 | 0.462 | 0.288 | 0.201 | 0.176 | 0.185 | 0.186 | 0.160 | 0.157 | 0.142 | 0.128 | 0.119 | 0.105 | 0.094 |
| 4.25 | 0.786 | 0.421 | 0.281 | 0.253 | 0.231 | 0.228 | 0.240 | 0.219 | 0.196 | 0.175 | 0.157 | 0.142 | 0.131 |
| 4.75 | 0.971 | 0.653 | 0.504 | 0.358 | 0.347 | 0.314 | 0.313 | 0.301 | 0.281 | 0.230 | 0.215 | 0.193 | 0.166 |
| 5.25 | 0.971 | 0.785 | 0.502 | 0.471 | 0.415 | 0.452 | 0.427 | 0.388 | 0.347 | 0.329 | 0.283 | 0.260 | 0.226 |
| 5.75 | 2.369 | 1.158 | 1.002 | 0.831 | 0.586 | 0.546 | 0.595 | 0.494 | 0.487 | 0.403 | 0.361 | 0.337 | 0.284 |
| 6.25 | 4.355 | 2.134 | 0.938 | 0.764 | 0.820 | 0.783 | 0.807 | 0.711 | 0.622 | 0.571 | 0.492 | 0.414 | 0.372 |

As Table 2 shows, the damage grows as $H_s$ increases and $T_p$ decreases. This trend correlates with the increase in steepness of the wave components for the FFT. A larger steepness generates larger velocities and accelerations, which ultimately leads to larger damage. In very few cases the basic trend cannot be observed. Possible reasons for this are the cancellation effects of the random phase shift that can play a role in dynamic analyses (Naess & Moan, 2013).

The proposed method assumes that the damage per year can be represented by an interpolated surface throughout the scatter. For the interpolation to take place only a few seastates are required to generate a surface that, with a certain margin of error, is able to reproduce similar results. This drastically reduces the number of seastates that need to be calculated. The interpolation is performed using a spline surface generated by the software tool MATLAB (2014).

In order to obtain an upper bound estimate of the possible reduction, nonlinear optimization techniques (Weicker, 2007) are used, which in this specific case are based on a Genetic Algorithm provided by MATLAB (2014). The objective is to remain within a specific margin of error while at the same time reducing the number of seastates that are needed to interpolate the planes. Results clearly show that only a few seastates are required. The result of one such analysis is shown in Table 3. The values marked in red are used to generate a spline surface while all remaining seastates are neglected.

**Table 3. Damage per year of worst hot spot, 0° direction, 1h analysis duration per seastate**

| | $T_p$[s] | | | | | | | | | | | | |
|---|---|---|---|---|---|---|---|---|---|---|---|---|---|
| $H_s$[m] | 5.5 | 6.5 | 7.5 | 8.5 | 9.5 | 10.5 | 11.5 | 12.5 | 13.5 | 14.5 | 15.5 | 16.5 | 17.5 |
| 0.25 | | | | | | | | | | | | | |
| 0.75 | | 0.003 | | | | 0.002 | | | | | | | |
| 1.25 | 0.038 | | 0.012 | 0.013 | 0.014 | 0.014 | 0.014 | 0.013 | 0.012 | | 0.010 | | |
| 1.75 | | 0.050 | 0.035 | 0.032 | 0.032 | 0.031 | 0.031 | 0.029 | 0.026 | | | | |
| 2.25 | | 0.091 | 0.063 | 0.055 | 0.058 | 0.056 | 0.052 | 0.050 | 0.045 | | | | |
| 2.75 | | 0.141 | 0.098 | 0.089 | 0.086 | 0.084 | 0.081 | 0.076 | 0.072 | 0.065 | | | |
| 3.25 | | | 0.151 | 0.126 | 0.126 | 0.122 | 0.119 | 0.109 | 0.104 | 0.093 | 0.085 | | |
| 3.75 | | | 0.201 | | 0.185 | 0.186 | 0.160 | 0.157 | 0.142 | 0.128 | 0.119 | | 0.094 |
| 4.25 | | | | | 0.231 | 0.228 | 0.240 | 0.219 | 0.196 | 0.175 | 0.157 | | |
| 4.75 | | | | | 0.347 | 0.314 | 0.313 | 0.301 | 0.281 | 0.230 | 0.215 | | |
| 5.25 | | | | | | 0.452 | 0.427 | 0.388 | 0.347 | 0.329 | | | |
| 5.75 | | | | | | | 0.595 | | | | | | |
| 6.25 | | | | | | | | | 0.622 | | | | |

Figure 13 visualizes Table 3 with the damage in the vertical axis. Figure 14 shows the interpolated damage surface using the red marked values only in comparison to the actual calculated values. The interpolated surface shown in Fig. 14 is a best fit overestimating the damage created by some seastates and underestimating others. The results of this optimization show that the necessary number of seastates, required to obtain accurate damage values can be drastically reduced.

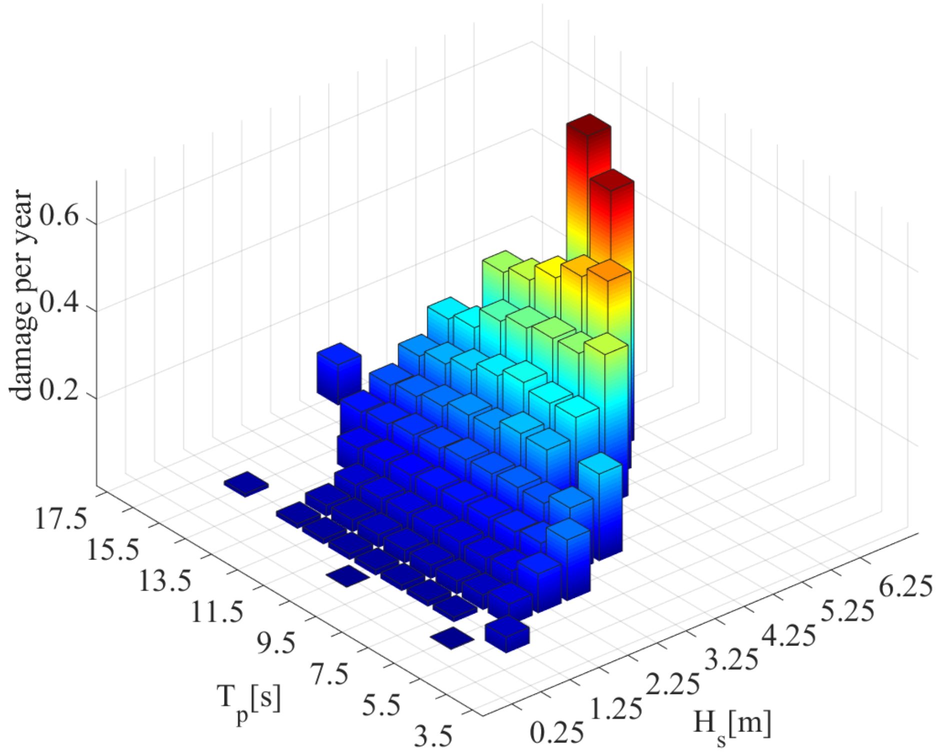


**Figure 13. Damage surface, worst hot spot, 0° direction, 1h simulation time**

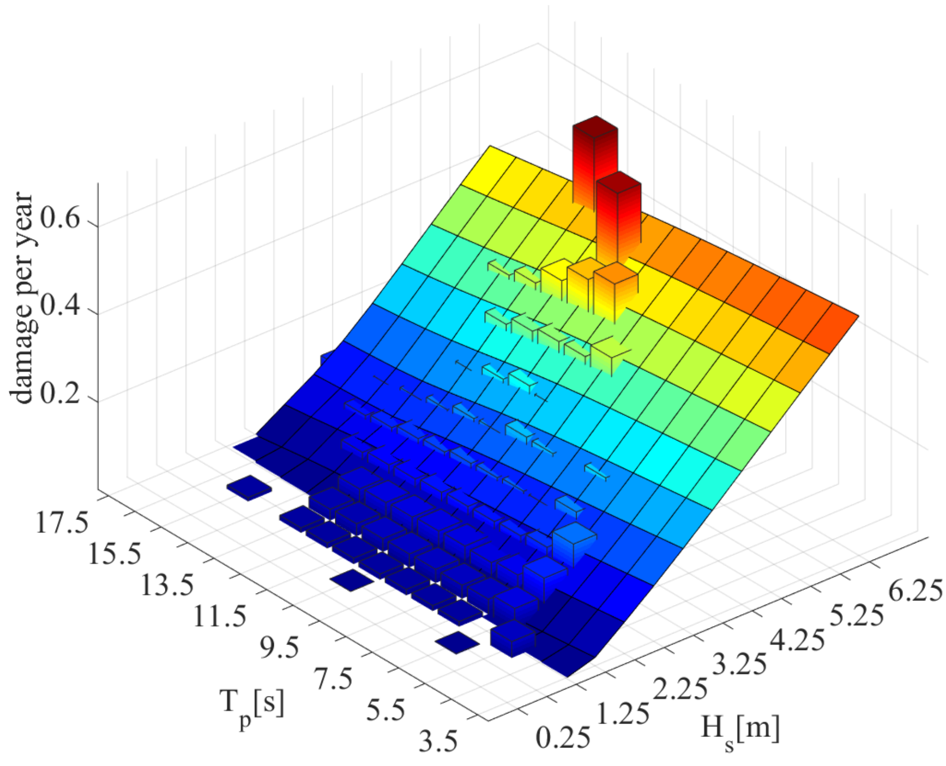


**Figure 14. Interpolated damage surface, worst hot spot, 0° direction, 1h simulation time**

On the other hand this information, resulting from a nonlinear optimization, provides no guidance on how to select which seastates should be used in order to obtain the interpolation surface. Therefore, a procedure is proposed based on a set of rules that will lead to a choice of seastates, whose corresponding interpolation surface will lead to an acceptable error margin.

## 4.2 Pattern to choose interpolation seastates

It is fair to assume that the seastates which possess a higher fraction of service life will have a larger impact on the total fatigue damage. The maximum fraction of wave life for each direction should therefore be the first choice for each direction. From this starting point it is possible to conceive four quadrants, indicated in Fig. 15, and assume that an additional point should be chosen in each quadrant.

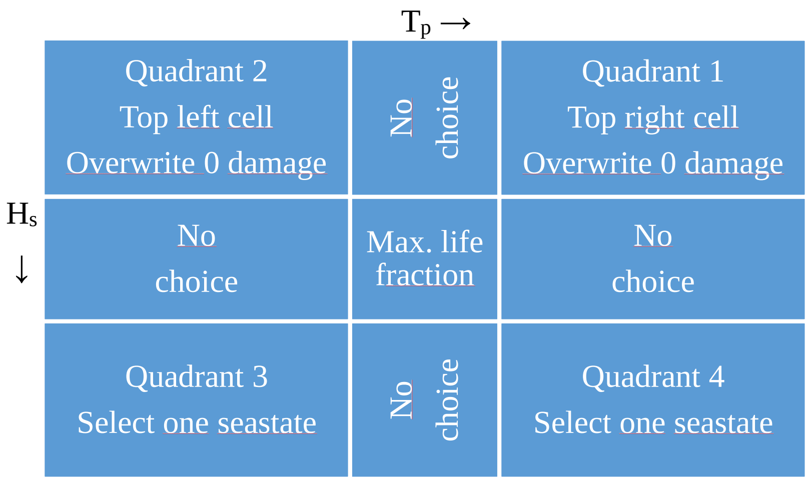


**Figure 15. Quadrant in the scatter diagram to select seastates for the interpolation**

Clearly, the first line of the damage surface will create very small damages. This is a valid assumption for a small $H_s$ (e.g. below one meter). Small waves would result in no fatigue damage at all or, in other words, a damage equal to zero. It is, therefore, recommended not to analyze these seastates and overwrite the damage plane with a zero at the top outer points of the scatter. With this assumption there remains only the need to choose seastates from the two bottom quadrants. This choice should be made based on how distant the seastates are from the central point and what their life fraction is. Results have shown that it is advantageous to select seastates that make up a higher fraction of service life even if they are adjacent to the seastate with the maximum life fraction.

An example of the described pattern is presented in Table 4 based on the same scatter diagram that is used for Table 3. The chosen seastates are marked with a red "X" and the quadrants are indicated by the blue background. The values in the line and the column of the seastate with the highest fraction of life are indicated by a "-" and are not part of the selection. The values presented with a black "x" are not used but could have been chosen under the proposed approach as well. It may be the case that the scatter does not include any seastates with a large $T_p$ and small $H_s$ in the top right of quadrant one, where the assumption of no damage is still valid. In this case, it can be helpful to artificially introduce a seastate with nearly no life fraction by manipulating the scatter. This is done in Table 4 for the seastate characterized by $T_p$=15.5sec. and $H_s$=0.75m. Comparing Table 4 and Table 3 shows that this seastate is not present in the measured scatter diagram.

**Table 4. Scatter diagram, 0° direction**

| | $T_p$[s] | | | | | | | | | | | | | |
|---|---|---|---|---|---|---|---|---|---|---|---|---|---|---|
| $H_s$[m] | 4.5 | 5.5 | 6.5 | 7.5 | 8.5 | 9.5 | 10.5 | 11.5 | 12.5 | 13.5 | 14.5 | 15.5 | 16.5 | 17.5 |
| 0.75 | | | **X** | | | | - | | | | | **X** | | |
| 1.25 | | x | | x | x | x | - | x | x | x | | x | | |
| 1.75 | | | x | x | x | x | - | x | x | x | | | | |
| 2.25 | | | x | x | x | x | - | x | x | x | | | | |
| 2.75 | | | - | - | - | - | **X** | - | - | - | - | | | |
| 3.25 | | | | x | **X** | x | - | x | x | x | x | x | | |
| 3.75 | | | | x | | x | - | x | **X** | x | x | x | | x |
| 4.25 | | | | | | x | - | x | x | x | x | x | | |
| 4.75 | | | | | | x | - | x | x | x | x | x | | |
| 5.25 | | | | | | | - | x | x | x | x | | | |
| 5.75 | | | | | | | | x | | | | | | |
| 6.25 | | | | | | | | | | x | | | | |

For specific cases of the two landside directions, where just a few seastates occur, it is more efficient to define a constant damage for the entire scatter diagram. Preferably this one seastate should have the highest fraction of service life. The result is a horizontal plane as the damage surface. For the other six directions, which have a sufficient number of seastates, this means that for each direction three seastates need to be analyzed, the seastate at the center, one at quadrant three and another at quadrant four. The result of this method is that instead of calculating the damage for all 331 seastates in the case of the sample platform this number could be reduced to 20, which is equivalent to a reduction of 94%. In order to test the robustness of this pattern a Monte Carlo simulation is performed, that chooses randomly seastates from the two bottom quadrants to generate the interpolated damage surface. The simulation is repeated 10.000 times. At each simulation a comparison is made with the analysis using all 331 seastates to determine how much the final damage deviates at the worst hot spots. The large number of simulations allows to generate distributions of the error in the calculation of the final damage. Figure 16 shows the empirical distribution of the damage of the worst 25 hot spots of the sample platform (blue lines) and an average distribution (black line).

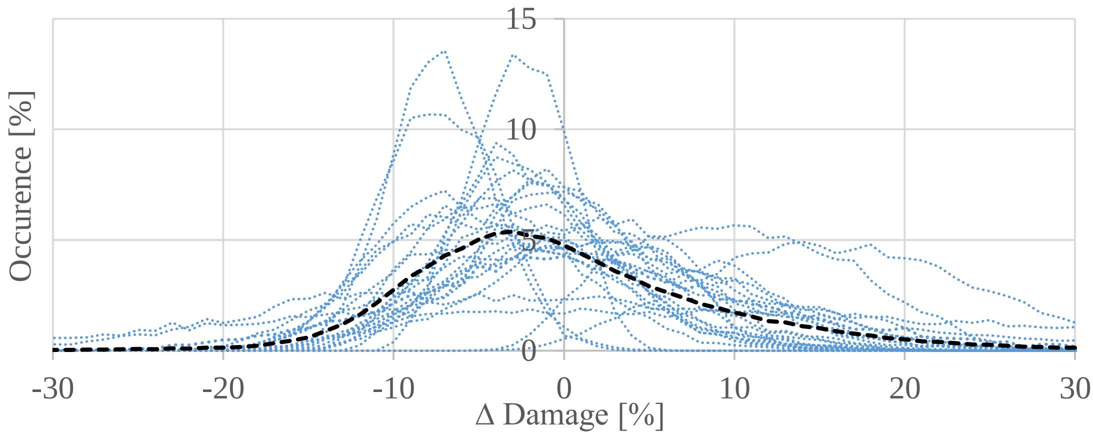


**Figure 16. Distribution of the damage for the worst 25 hot spots using Monte Carlo simulation**

Although the simulation chooses randomly different seastates at each simulation, the final damage is very similar. This is shown by the narrow distribution in Fig. 16 which has its support between −15% to +15%. This means that independent of the choice of the seastates that needed to be analyzed in quadrants three and four, the interpolated damage surface generates reasonable results within an error margin of ±15%. The procedure is quite robust and does not depend on a specific choice of seastates. The engineer performing the task can choose any seastate in the specified quadrants and still determine results within an acceptable error margin.

## 5 CONCLUSION

Although time domain analyses are generally accepted to be the most accurate method of determining the fatigue life of a structure, they are at the same time computationally demanding and have so far remained infeasible. Therefore, this paper proposes a novel approach that drastically reduces the computational effort while maintaining a high level of accuracy. Instead of calculating the damage caused by all seastates, the proposed method interpolates the damage caused by various seastates in a scatter diagram and shows that only a small number of seastates need to be analyzed in order to obtain an accurate solution. In addition, this paper determines the parameters required to perform an accurate time domain fatigue analysis of a jacket structure. The key parameters, such as the number of frequency components for the Fourier Transform, duration of the simulated time, and the choice of seed, are investigated for the specific case of offshore jackets. Taken together this paper achieves a substantial reduction in computational effort required and hence makes the time domain method a feasible alternative for a design project or a revaluation study of older platforms.

## REFERENCES

ABS, 2014. *Guide For Fatigue Assessment of Offshore Structures,* Houston: American Bureau of Shipping.

Anderson, T., 2005. *Fracture Mechanics Fundamentals and Applications.* 3 ed. Boca Raton: Taylor & Francis Group, LLC.

API, 2007. *API Recommended Practice for Planning, Designing and Constructing Fixed Offshore Platforms - Working Stress Design RP 2A-WSD,* Washington: API Publishing Services.

Barltrop, N. & Adams, A., 1991. *Dynamics of Fixed Marine Structures.* 3 ed. Oxford: Butterworth-Heinemann Ltd.

BSI, 2013. *BS 7910 Guide to methods for assessing the acceptability of flaws in metallic structures.* 3 ed. s.l.:British Standard Institution Standards Limited.

Chakrabarti, S. K., 2005. *Handbook of Offshore Engineering.* London: Elsevier.

DNV, 2011. *DNV-RP-H103 Modelling and Analysis of Marine Operations,* s.l.: Det Norske Veritas AS.

DNVGL, 2014. *Recommended Practice Fatigue design of offshore steel structures DNVGL-RP-0005:2014-06 ,* s.l.: DNV GL AS.

Dowling, N. E., 1999. *Mechanical Behavior of Materials.* New Jersey: Prentice-Hall, Inc.

Efthymiou, M., 1988. Development of SCF Formulae and Generalized Influence Functions for Use in Fatigue Analysis. *OTJ 88 Proceedings of the Conference on recent developments in tubulat joints technology,* 4th October, pp. 2-1 to 2-33.

Hasselmann, K. et al., 1973. *Measurement of Wind-Wave Growth and Swell Decay during the Joint North Sea Wave Project (JONSWAP),* Hamburg: Deutsches Hydrographisches Institut.

ISO, 2013. *International Organization for Standardization - Petroleum and natural gas industries - Fixed steel offshore structures (ISO19902:2007+Amd 1:2013),* Brussels: CEN.

Jia, J., 2008. An efficient nonlinear dynamic approach for calculating wave induced fatigue damage of offshore structures and its industrial applications for lifetime extension. *Applied Ocean Research*, 6 November, pp. 189-198.

Lassen, T. & Recho, N., 2006. *Fatigue Life Analysis of Welded Structures.* London: ISTE Ltd.

Marshall, P. W., 1992 . *Design of Welded Tubular Connections.* Amsterdam: Elsevier Science Publishers B.V.

MATLAB , 2014. *MATLAB.* R2014 ed. Natick, Massachusetts: The MathWorks, Inc..

Morison, J., 1953. *The Force Distribution Exerted by Surface Waves on Piles, Technical Report Series 3, Issue 345,* Berkeley: University of California, Institute of Engineering Research.

Naess, A. & Moan, T., 2013. *Stochastic Dynamics of Marine Structures.* New York: Cambridge University Press.

Palmgren, A., 1924. Die Lebensdauer von Kugellagern. *VDI-Zeitschrift* , Volume 58, pp. 339-341.

Sarpkaya, T., 2010. *Wave Forces on Offshore Structures.* New York: Cambridge University Press.

Sorensen, R. M., 2006. *Basic Coastal Engineering.* 3rd ed. New York: Springer Science+Business Media Inc.

USFOS, 2010. *Usfos Hydrodynamics Theory Description of use Verification.* Sandsli, Norway: USFOS A/S.

Weicker, K., 2007. *Evolutionäre Algorithmen.* Wiesbaden: Teubner.